14th International Symposium on Turbulence and Shear Flow Phenomena (TSFP14)
Heidelberg, Germany, July 28–31, 2026

WAKE-INDUCED TRANSITION IN SEPARATED BOUNDARY LAYERS

Maziyar Hassanpour
Mechanical and Manufacturing Engineering
University of Calgary
AB T2N 1N4, Canada
maziyar.hassanpour@ucalgary.ca

Robert J. Martinuzzi
Mechanical and Manufacturing Engineering
University of Calgary
AB T2N 1N4, Canada
rmartinu@ucalgary.ca

Ugo Piomelli
Mechanical and Materials Engineering
Queen's University
ON K7L 3N6, Canada
ugo@queensu.ca

ABSTRACT

We investigate wake-induced transition to turbulence in a laminar boundary layer over a flat wall using direct numerical simulation (DNS). The wake is generated by a circular cylinder of diameter D placed near the wall at a moderate gap ratio. The Reynolds number is $Re_D = DU_\infty/\nu = 3900$, with U_∞ being the free-stream velocity and ν the kinematic viscosity. Energy transfer is analyzed within a modal framework that combines proper orthogonal decomposition and wavelet-based spectral decomposition (wPOD), enabling scale-resolved identification of coherent motions and their interactions. Disturbance amplification first occurs at slow, large scales associated with wall shear-layer flapping. The dominant turbulent kinetic energy (k) production appears downstream at the primary shedding scale during the formation of the wall roller. These wall rollers deform into Λ-vortices whose shedding redistributes k away from the production region through pressure-driven transport mechanisms. Subsequently, triadic interactions transfer energy to smaller scales, promoting broadband spectral redistribution and the progressive development of turbulence. Pressure-mediated processes associated with the self-sustaining wall-cycle then organize and redistribute the streaky structures beneath the Λ-vortices, reinforcing the breakdown process in the next shedding cycle.

1 Introduction

This work investigates transition in a separated laminar boundary layer (SLB). Previous studies have focused on natural transition in SLBs (Spalart & Strelets, 2000; Jaroslawski *et al.*, 2023), whereas this work examines the wake-induced case. The study tracks energy cascade from its generation site through nonlinear harmonics, to the dissipative scales, thereby delineating the successive stages of breakdown. Each transition stage can be linked to a spectral signature, thus providing a basis for flow control.

Spalart & Strelets (2000), motivated by the relevance of SLB transition to the loading of aircraft wings, investigated transition in a SLB triggered by weak free-stream turbulence (FST) and documented the early stages of natural transition. They showed that transition begins when a SLB flapping motion amplifies disturbances. This motion destabilizes the separated shear layer. Once the instability reaches a critical amplitude, transition occurs abruptly and the flow then reattaches.

In many practical configurations, such as wings with leading-edge slats or turbomachinery blades, transition in a SLB is triggered by wake interactions. By examining wake-induced transition at low $Re_\theta = 175$, where θ is the boundary-layer momentum thickness, Hassanpour *et al.* (2025) identified key differences from FST-driven transition. In FST-induced cases, instabilities amplify at their natural frequencies. In wake-induced transition, however, the boundary layer is forced at the characteristic wake shedding frequency, f_v. Unlike the abrupt breakdown reported by Spalart & Strelets (2000), the wake-induced process occurs over several D.

This gradual development occurs with the emergence of Λ-vortices, characteristic of K-type natural transition, organized into aligned structures within the separated shear layer (Kachanov, 1994). Hassanpour *et al.* (2025) presented evidence that the formation and shedding of these Λ-vortices involve superharmonic resonance. In this process spectral energy at fv is redistributed to higher harmonics $2f_\mathrm{v}$ and $3f_\mathrm{v}$ during Λ-vortex formation and shedding.

This work addresses the dynamics underlying the spectral energy transfer and the spectral characteristics of each transition stage. A modal framework is used here to characterize the underlying processes and delineate the flow spectral evolution in successive stages of transition.

2 Methods

The DNS model is developed in Nektar++ (Cantwell *et al.*, 2015), using a spectral element method. The computational model has 226×10^6 degrees of freedom, with a polynomial order of 12 in the spectral element discretization and a Fourier expansion in the spanwise direction with 92 Fourier planes. This resolution was found to give grid convergence (Hassanpour *et al.*, 2025).

To characterize the transition process, we identify coherent motions that exhibit nearly harmonic behavior. The frequency and amplitude of these motions vary in time; but, their energy remains concentrated around a central frequency, with the spectral energy density decaying rapidly away from it. Such motions can be approximated as harmonic, self-sustained oscillations with slowly varying amplitude and frequency.

From analytic-signal theory, such a representation corresponds to a *monocomponent* signal, defined as one possessing a positive instantaneous frequency $\omega(t)$ that varies slowly in time, such that $\dot{\omega}(t)/\omega^2(t) \ll 1$. These signals are expressed as complex-mode pairs, $a_i(t) = A(t)\mathrm{cis}\left(\int_0^t \omega(\tau)\,d\tau + \phi\right)$, where $\mathrm{cis}(x) = \cos x + i \sin x$ and $A(t)$ is a slowly varying amplitude. In this formulation, the convective character of vortex shedding is associated with the $\pi/2$ phase shift between paired modes.

POD analysis is well suited for periodic wakes because vortex shedding typically carries more energy than other convective instabilities (Noack *et al.*, 2011). In POD, the velocity field is decomposed as $u(\mathbf{x},t) = \sum_i \phi_i(\mathbf{x})\, a_i(t)$, where $\phi_i(\mathbf{x})$ are spatial modes and $a_i(t)$ are the corresponding temporal coefficients. An energetic monocomponent motion centered at f_v is isolated as the leading POD mode pair.

In wake-induced transition, motions at harmonics of f_v also contribute to the transition to turbulence (Hassanpour *et al.*, 2025). While POD effectively extracts the primary shedding as a monocomponent mode pair, the POD modes associated with $2f_\mathrm{v}$ and $3f_\mathrm{v}$ often exhibit spectral contamination. This nonmonocomponent quality complicates the identification of dyadic and triadic interactions and obscures the energy transfer pathways that characterize the transition to turbulence.

Extracting these motions as monocomponent pairs requires a suitable separation of temporal scales. We introduce a hybrid framework combining POD and orthogonal wavelet analysis (wPOD). The strategy begins by applying POD to the velocity and pressure fields, extracting the leading mode pair that captures the primary shedding dynamics at f_v. To recover modes of shedding harmonics: (i) temporal bandpass filtering via the maximal overlap discrete wavelet transform with multiresolution analysis (MODWT-MRA) (Percival & Walden, 2000) is applied to the residual fields at each point, generating frequency bins with controlled cutoff frequencies; (ii) POD in the bins centered at f_v, $2f_\mathrm{v}$, and $3f_\mathrm{v}$ is performed to extract monocomponent mode pairs.

Within the frequency bins associated with f_v (note that after extracting the first POD mode pair, the residual field still retains spectral energy around f_v), $2f_\mathrm{v}$, and $3f_\mathrm{v}$, the temporal coefficients of the leading POD mode pair exhibit spectral energy concentrated at a well-defined central frequency, visible as a dominant peak in the spectrum. Energy content in sidebands about the central frequency indicate that the primary oscillation is not strictly monochromatic but undergoes slow amplitude and/or frequency modulation. In other words, the coherent motions at f_v, $2f_\mathrm{v}$, and $3f_\mathrm{v}$ are modulated by a lower-frequency process that redistributes spectral energy.

The MODWT–MRA filter parameters are selected objectively based on two key parameters that define the spectral partitioning. First, the number of bins determines how the frequency spectrum is divided into intervals. Second, the edge sharpness controls how abruptly the filter transitions between adjacent frequency bins. Low sharpness allows greater overlap and frequency mixing between neighboring bins, whereas high sharpness enforces a more distinct separation with reduced mixing. These parameters are tuned such that the resulting POD mode pairs for the bins centered at f_v, $2f_\mathrm{v}$, and $3f_\mathrm{v}$ approach monocomponent behavior. As a result, coherent periodic motions retain as much turbulent kinetic energy within a mode as possible within their designated frequency interval and exhibit nearly monocomponent properties.

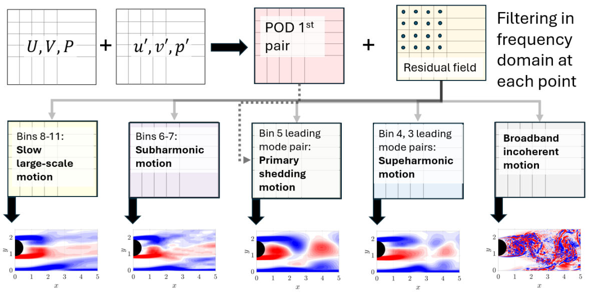

Figure 1: Workflow of the wPOD methodology, illustrating the sequential steps from wavelet-basedn decomposition into discrete frequency bins to POD performed within each bin.

Once monocomponent mode pairs are isolated, the energetic mechanisms governing transition can be examined within a modal framework. The flow field is decomposed as

$$\begin{aligned}\begin{bmatrix} u(\mathbf{x},t) \\ v(\mathbf{x},t) \end{bmatrix} &= \begin{bmatrix} U(\mathbf{x}) \\ V(\mathbf{x}) \end{bmatrix} + \sum_{k=1}^{2} a_k(t) \begin{bmatrix} \Phi_{u,k}(\mathbf{x}) \\ \Phi_{v,k}(\mathbf{x}) \end{bmatrix} \\ &\quad + \sum_{j=1}^{J} \sum_{n=1}^{N} a_n^{(j)}(t) \begin{bmatrix} \Phi_{u,n}^{(j)}(\mathbf{x}) \\ \Phi_{v,n}^{(j)}(\mathbf{x}) \end{bmatrix}, \end{aligned} \tag{1}$$

where U and V denote the mean velocity components. The first summation corresponds to the leading POD mode pair associated with the fundamental shedding frequency f_v. The second summation contains modes extracted from a wavelet-based decomposition (bins) of the residual field after removal of the fundamental pair. The residual signal is partitioned into $J = 11$ discrete frequency bins using wavelet filtering. POD is then applied independently within each bin. The parameter N denotes the number of modes retained in each bin. This hybrid procedure constitutes wPOD. It enables the isolation of spectrally compact, nearly monocomponent structures across multiple scales in an objective way.

The wPOD workflow and motions contained in the different bins are illustrated in Fig. 1. The slow large-scale motions are contained in Bins 8 to 11, while bins 6 and 7 contain subharmonic motions. Bands 6 and 7 correspond to subharmonic components. Bin 5 is centered at f_v, representing coherent shedding dynamics not captured by the first POD mode pair. The leading modes of bins 3 and 4 correspond to the superharmonic frequencies $2f_\mathrm{v}$ and $3f_\mathrm{v}$, respectively. The remainder of the flow field contains incoherent motion.

To obtain a dynamically meaningful representation, related modes are grouped based on their spectral content. Modes with central frequency f_v are grouped as *primary shedding mode*. The modes associated with $2f_\mathrm{v}$ and $3f_\mathrm{v}$, are grouped as the *superharmonic mode*. The modes of bins 6 and 7 are grouped as the *subharmonic modes*, while the slow-frequency bins (bins 8–11) constitute the *slow mode*. The remaining contributions, consisting of higher-order modes and unresolved residual content across all bands, are grouped and defined as the *incoherent mode*.

The velocity field is reconstructed and the contributions of the five motions to the k-transport in (2) are identified. Here, $\mathscr{P}$ denotes production, ε dissipation, $\mathscr{T}_j$ the triple-correlation transport, and Π_j the pressure–velocity correlation transport.

$$\frac{Dk}{Dt} = \mathscr{P} - \varepsilon - \frac{\partial \mathscr{T}_j}{\partial x_j} - \frac{\partial \Pi_j}{\partial x_j} + \nu \frac{\partial^2 k}{\partial x_j^2}, \qquad (2)$$

Substituting the five-component decomposition into (2) gives rise to dyadic and triadic interaction terms. The dyadic contributions—such as the Reynolds stresses appearing in the production, advection, and pressure-transport terms—formally yield $5 \times 5 = 25$ pairwise combinations among the five motions. Each transport term can therefore be expressed as a sum of interactions between all possible pairs of the decomposed velocity components.

However, the motions are spectrally separated by construction. Components such as the slow and subharmonic motions do not share common frequency support. Consequently, most cross-products arising from the above expansion are exactly or nearly orthogonal in time and therefore yield negligible net contribution upon averaging. For example, a cross-term such as $u_{\text{slow}}u_{\text{primary}}$ (u_{slow} and u_{primary} are slow and primary velocity fields, respectively) does not produce a significant contribution to production. In contrast, self-interaction terms such as $u_{\text{slow}}u_{\text{slow}}$ or $u_{\text{primary}}u_{\text{primary}}$ directly contribute to production. This spectral orthogonality substantially reduces the number of dynamically relevant interaction pathways, despite the larger number of formally possible terms.

The triple-correlation transport term produces triadic interactions, formally yielding $5^3 = 125$ possible combinations. However, due to spectral separation, only triads satisfying the Fourier-type condition $f_i \pm f_j \pm f_k = 0$ survive temporal averaging. Thus, combinations such as $(f_{\text{primary}}, f_{\text{primary}}, -2f_{\text{primary}})$—or, more generally, harmonically related interactions (e.g., primary–primary–superharmonic)—contribute, whereas frequency-mismatched triads vanish.

In addition, dyadic and triple correlation terms involving the broadband incoherent component may also contribute, as its wide spectral support enables frequency matching with multiple combinations. Consequently, these interactions govern inter-scale energy redistribution during transition.

3 Results

We first examine the overall flow dynamics through analysis of the vorticity field and the associated vortex evolution. We then perform a modal decomposition to identify the underlying spatiotemporal coherence and characterize the dominant modal dynamics. In this section, we focus on the primary and superharmonic motions in order to highlight the differences between wPOD and conventional POD representations. Finally, in the energy-transition analysis, we quantify and discuss the contribution of each class of motion—defined previously in the Methods section—to the transition process.

3.1 General dynamics

The flow vorticity field is shown in Fig. 2a and 2b. The wake exhibits: Kármán vortex shedding (high-vorticity regions: UR and LR) from the cylinder and the periodic formation and shedding of a wall roller (high-vorticity regions: WR). During one shedding cycle, the boundary layer separates at $x \approx 0.5$, rolls up at $x \approx 1$, and subsequently deforms into a Λ-vortex (high-vorticity regions: Λ_1) from $x \approx 2$ to $x \approx 4$. Beneath this Λ-vortex structure (Fig. 2c), streaky structures (Fig. 2d) emerge at $x \approx 2$ to 4. As the Λ-vortex convects downstream, it interacts with the overlying wake vortices and the underlying streaks. These interactions promotes break down of Λ-vortex at $x \approx 5$ (Λ_2 in Fig. 2b).

Finally, the Λ_2-vortex fragments into streamwise-oriented vortical structures, marking the completion of transition. The residual streaks persist beyond the initial fragmentation event and continue to interact downstream, thereby sustaining and closing the near-wall cycle (Waleffe, 1997; Jiménez & Pinelli, 1999) as discussed in Hassanpour *et al.* (2025).

3.2 Modal analysis

The fundamental shedding spatial modes (only mode 1 of pair), $\Phi_u^{f_v}$ and $\Phi_v^{f_v}$, are shown in Fig. 3a and Fig. 3b. These modes contain two convective waves: one corresponding to Kármán vortex-shedding in the wake and the other developing within the separated boundary layer (see the gray rectangle in Fig. 3). The coexistence of wake forcing and boundary-layer response within a single coherent spatial structure indicates phase locking between the wake and the coherent energetic dynamics within the separated shear layer. This phase locking implies a dynamically coupled system in which the wake shedding synchronizes the shedding within the separated boundary layer, thereby governing the progression of transition. Such lock-on provides sustained external forcing that regulates instability amplification, helping to explain why wake-induced SLB transition proceeds gradually, in contrast to the abrupt breakdown typical of FST-driven transition.

The spectra of the temporal coefficients, $a_1^{f_v}(t)$ and $a_2^{f_v}(t)$ in Fig. 3c are identical and centered at the shedding frequency f_v, indicating that the mode pair represents a single coherent oscillatory process. The phase portrait of $a_1^{f_v}(t)$ and $a_2^{f_v}(t)$ in Fig. 3d indicates that the two modes form a conjugate pair representing the quadrature components of a harmonic oscillator at f_v, with weak amplitude modulation.

The first harmonic leading spatial modes (wPOD mode 1 of bin 4), $\Phi_u^{2f_v}$ and $\Phi_v^{2f_v}$, are shown in Fig. 4a,b, while mode 2 exhibits a similar spatial topology and comparable energy. The corresponding spectra of temporal coefficients, $a_1^{2f_v}(t)$ and $a_2^{2f_v}(t)$, are presented in Fig. 4c,d. Both spectra are centered at $2f_v$, and the phase portrait forms a closed doughnut-shaped limit cycle. Taken together, these results indicate that the $2f_v$ content is captured as a conjugate, harmonically related mode pair.

As in the fundamental mode, the spatial structures display two convective wave packets: one associated with the wake and the other developing along the wall within the separated boundary layer. The coexistence of wake and wall signatures within a single coherent structure indicates that the $2f_v$ response remains phase locked to the primary shedding.

The leading $3f_v$ spatial modes, $\Phi_u^{3f_v}$ and $\Phi_v^{3f_v}$ (Fig. 5), exhibit features similar to the $2f_v$ case, with paired wake–wall structures, spectra centered at $3f_v$, and a closed phase portrait. Figure 5 thus confirms that the superharmonic content forms a conjugate, harmonically related mode pair phase-locked to the primary shedding process.

Bin 5 is also centered at f_v and yields a second mode pair at the fundamental frequency (Fig. 6). Although its spectra and phase portrait confirm monocomponent, oscillator-like behavior similar to the primary shedding pair, the spatial structures differ in their organization and localization. The presence of two distinct mode pairs at f_v therefore reflects separate coherent motions differing in spatial organization and dynamical role and should not misinterpreted as noise contamination.

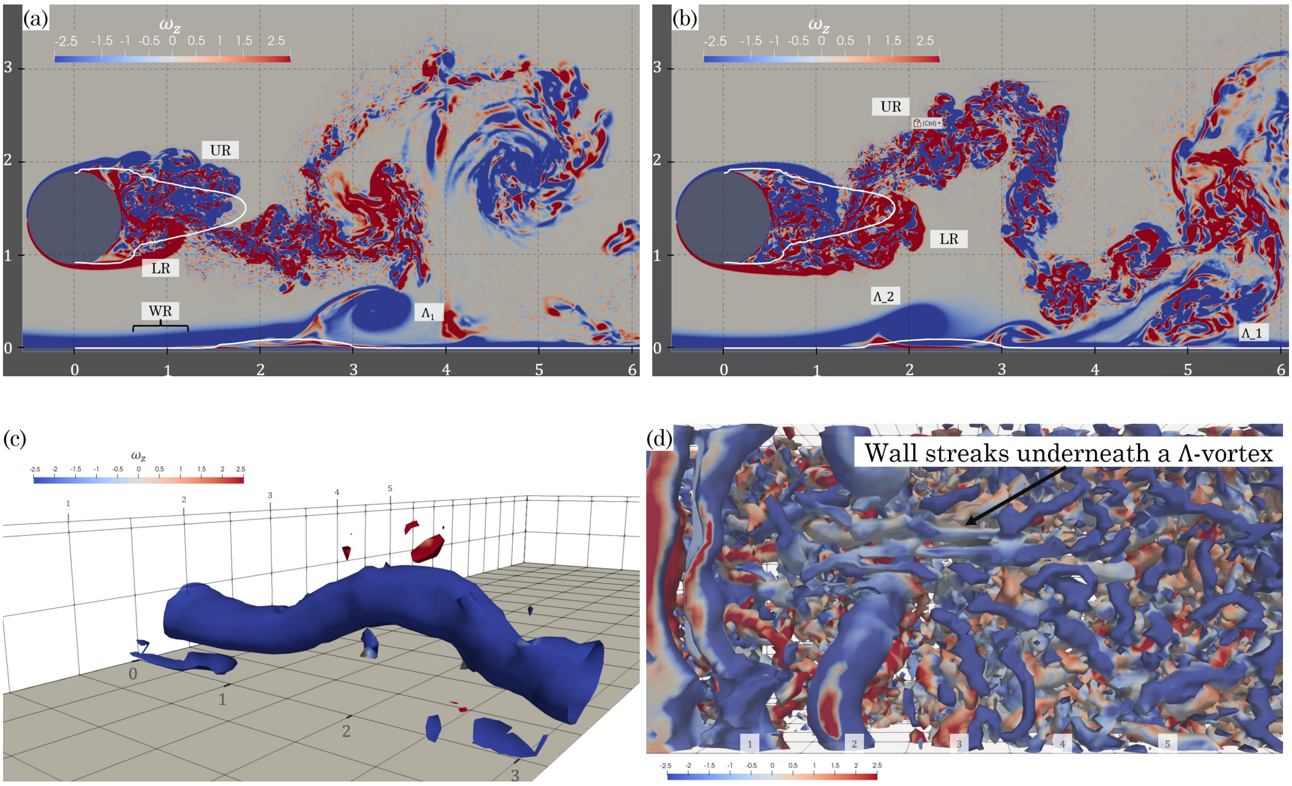

Figure 2: Instantaneous vorticity field illustrating wake–boundary-layer interactions. (a) Instant when the upper wake vortex (UR), with negative sense of rotation, is shed from the cylinder. (b) Instant when the lower wake vortex (LR), with positive sense of rotation, is shed. (c) Q-criterion isosurfaces showing the isolated Λ-vortex. (d) Q-criterion isosurfaces highlighting the formation of streaky structures.

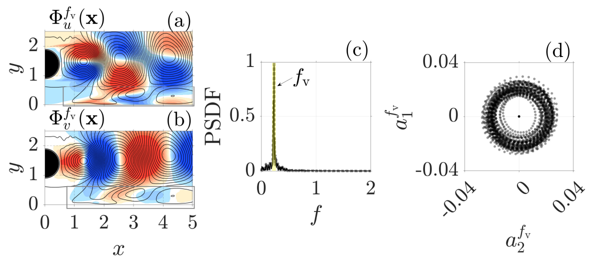

Figure 3: Leading f_v primary shedding mode pair (mode 1 of the wPOD pair, identical to POD): (a,b) spatial structures $\Phi_u^{f_\mathrm{v}}$ and $\Phi_v^{f_\mathrm{v}}$ (gray box indicates wall dynamics phase-locked to the wake); (c) spectra of $a_1^{f_\mathrm{v}}$ (solid) and $a_2^{f_\mathrm{v}}$ (dotted); (d) phase portrait.

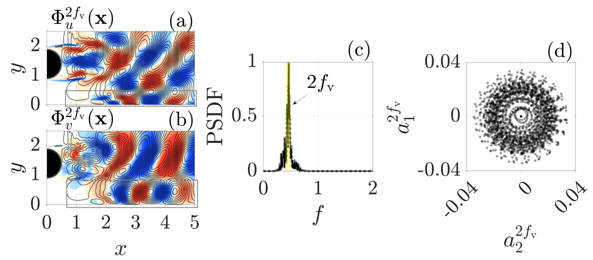

Figure 4: Leading $2f_\mathrm{v}$ primary shedding mode pair (mode 1 of the wPOD pair in bin 4): (a,b) spatial structures $\Phi_u^{2f_\mathrm{v}}$ and $\Phi_v^{2f_\mathrm{v}}$ (gray box indicates wall dynamics phase-locked to the wake); (c) spectra of $a_1^{2f_\mathrm{v}}$ (solid) and $a_2^{2f_\mathrm{v}}$ (dotted); (d) phase portrait.

The reconstructed instantaneous vorticity field, obtained from the mean flow together with the fundamental, its superharmonics, and the additional f_v mode, is shown in Fig. 7. This reconstruction isolates the organized shedding dynamics. Superimposed on this field are vorticity isocontours reconstructed using only the mean flow and the first leading POD mode. The comparison demonstrates that incorporating the harmonic content reorganizes the vorticity distribution (see the zoomed-in section). Moreover, a comparison between the filled color contours (harmonically enriched reconstruction) and the line contours (mean plus first POD mode) shows improved agreement with instantaneous field not only in spacing but also in vortex morphology. Thus, the inclusion of harmonics refines the spatial representation of the shedding motion and captures its multi-scale organization with greater fidelity.

The role of the slow scales is similar to what reported by Najjar & Balachandar (1998). The slow scales introduce a cyclic expansion and contraction of the vorticity formation region, corresponding to a low-frequency modulation of the shedding process. Subharmonic motions (not shown) further refine the near-wall high-vorticity topology—particularly the wall roller and Λ-vortex—by improving the representation of their deformation and spatial organization.

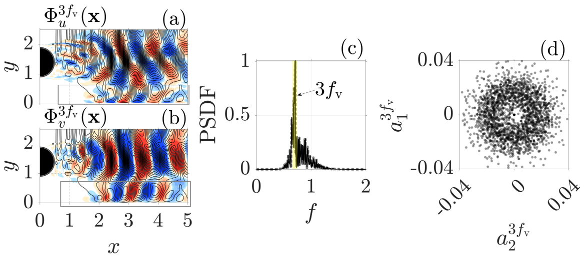

Figure 5: Leading $3f_\mathrm{v}$ primary shedding mode pair (mode 1 of the wPOD pair in bin 3): (a,b) spatial structures $\Phi_u^{3f_\mathrm{v}}$ and $\Phi_v^{3f_\mathrm{v}}$ (gray box indicates wall dynamics phase-locked to the wake); (c) spectra of $a_1^{3f_\mathrm{v}}$ (solid) and $a_2^{3f_\mathrm{v}}$ (dotted); (d) phase portrait.

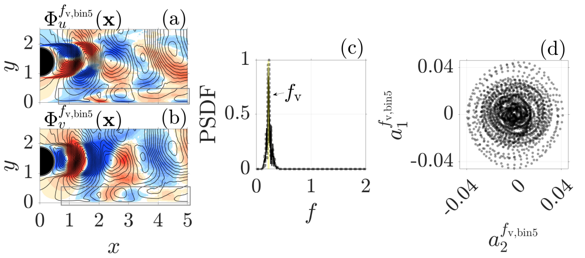

Figure 6: Leading f_v primary shedding mode pair (mode 1 of the wPOD pair in bin 5): (a,b) spatial structures $\Phi_u^{f_\mathrm{v}}$ and $\Phi_v^{f_\mathrm{v}}$ (gray box indicates wall dynamics phase-locked to the wake); (c) spectra of $a_1^{f_\mathrm{v}}$ (solid) and $a_2^{f_\mathrm{v}}$ (dotted); (d) phase portrait.

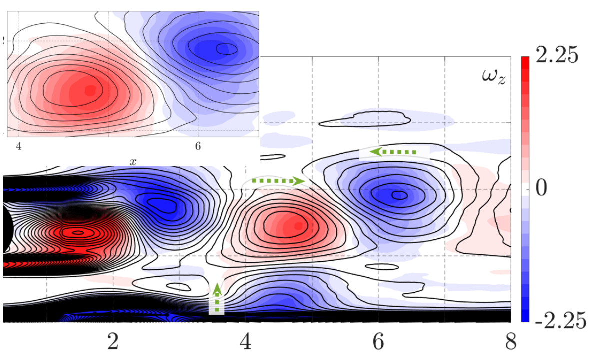

Figure 7: Instantaneous reconstructed vorticity field: contour lines show the reconstruction using the mean flow and the first POD mode pair at f_v; colored contours include the addition of the superharmonics ($2f_\mathrm{v}$, $3f_\mathrm{v}$) and the f_v mode from bin 5.

3.3 Transition dynamics

We begin the discussion of the transition process by examining the streamwise distribution of production. An inspection of all modal production maps indicates that the dominant contributions arise from the slow motions, the fundamental shedding mode, and the incoherent component, primarily through their dyadic self-interactions. Production due to these contributions, shown in Fig. 8, form the basis of the following analysis.

At the slow scales, production emerges early within the separated shear layer over $\sim 0.5 < x <\sim 1.5$, as shown in

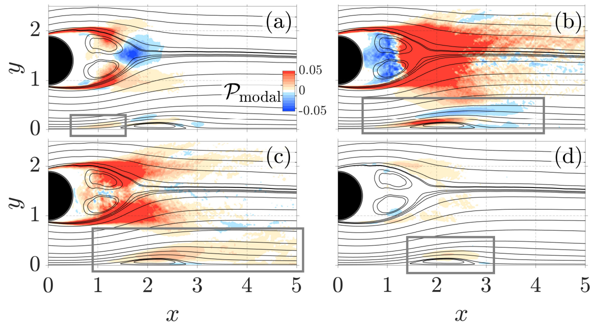

Figure 8: Production maps illustrating the contributions from different modal interactions: (a) slow–slow interaction, (b) primary shedding–primary shedding interaction, (c) superharmonic–superharmonic interaction, and (d) incoherent–incoherent interaction.

Fig. 8a. In this region, the dynamics are characterized by a large-scale flapping motion (Spalart & Strelets, 2000; Hassanpour *et al.*, 2025). This slow motion is introduced to the shear layer by the wake's global breathing dynamics.

Farther downstream, the large production rate occurs over $\sim 1 < x <\sim 2.5$ (Fig. 8b) and is associated with amplification at the fundamental shedding frequency, f_v. This region coincides with the roll-up of the wall roller. The spatial overlap between peak production and coherent vortex formation highlights the role of the primary shedding mode as the main energy-transfer mechanism, converting mean shear into organized vortical structures that drive the transition process.

Beyond $x \approx 1.5$, incoherent production (Fig. 8c) emerges and peaks downstream of $x \approx 2.5$, following the decay of the fundamental-scale contribution. This production coincides with the deformation of the wall roller into a Λ-vortex. In this region, intensified velocity gradients and strain redistribute energy is being transferred from the organized highly coherent large-scale motions to smaller scales and losing coherence.

In the intermediate region, $\sim 2 < x < \sim 3$, superharmonic modes ($2f_\mathrm{v}$ and $3f_\mathrm{v}$) contribute weakly production (Fig. 8d), indicating that these harmonics directly extract energy from the mean flow once established.

Three mechanisms govern the redistribution of k within the SLB and thereby facilitate the subsequent stages of transition: convection, pressure–velocity correlation, and the triple-correlation term. The convection and pressure–velocity correlation terms redistribute k spatially without altering its spectral content. In contrast, the triple-correlation term, which arises from triadic interactions mediates inter-scale energy transfer.

The pressure–velocity correlation term is shown in Fig. 9. The contribution from the slow large scales is weak but extends along the SLB (Fig. 9a). In contrast, at the fundamental shedding scale, f_v and incoherent scales, the pressure–velocity term becomes significant centered at $x \approx 2$ (Fig. 9b,c). Within the separated shear layer it is predominantly negative, implying a redistribution of k away from the local production region. Beneath the separated layer, where streaky structures develop, the contribution changes sign and becomes positive.

The transfer of k to smaller scales as transition progresses can be traced through the triple-correlation terms (Fig. 10), which quantify triadic energy exchange among the modal components. These maps reveal a streamwise sequence of scale interactions accompanying the development of instability.

The interaction involving the slow large-scale motion is active within the separated shear layer and upstream of vortex

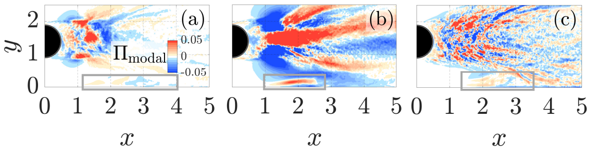

Figure 9: Pressure-velocity correlation maps associated with the self-interaction of (a) slow-scale motion, (b) primary shedding at f_v, and (c) incoherent components. The gray box indicate where interaction is occurring for each motion.

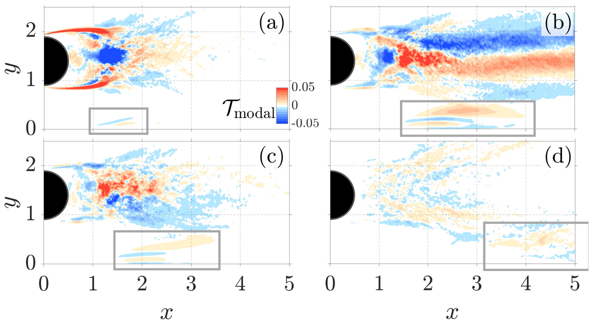

Figure 10: Triple-correlation maps illustrating triadic interactions among (a) slow–primary–primary motions, (b) primary–primary–superharmonic motions, (c) primary–primary–incoherent motions, and (d) subharmonic–subharmonic–incoherent motions. The gray boxes highlight the streamwise regions where each interaction is most active.

roll-up, over $1 < x < 2$. In this region, where flapping dynamics are observed (Fig. 10a), the dominant triad is primary shedding–primary shedding–slow motion. This interaction reflects a redistribution of energy from the initial large-scale amplification toward the fundamental instability.

The strongest triadic contributions involve the fundamental mode and are concentrated near the location where the wall-attached roller deforms into a Λ-vortex and subsequent shedding occurs at $x \approx 2$ to $x \approx 4$. In particular, the fundamental–fundamental–superharmonic (Fig. 10b) and fundamental–fundamental–incoherent interactions (Fig. 10c) represent the transfer of energy from the shedding frequency to higher harmonics and to incoherent motions in this region.

This redistribution accompanies the deformation of the wall-attached roller into Λ-vortices and their alignment into organized rows, consistent with the onset of K-type transition. The superharmonic interactions reflect continued harmonic amplification through this mechanism, whereas the incoherent interactions mark the initial stages of breakdown toward broadband turbulence and are not examined further here.

Farther downstream, the subharmonic motions interact primarily with the incoherent component through subharmonic–incoherent triads (Fig. 10d). These interactions are active over $3 < x < 5$, where convection at these scales is also observed, indicating their involvement in the later stages of transition characterized by broadband energy redistribution.

4 Concluding remarks

This work provides a detailed characterization of wake-induced transition within a separated laminar boundary layer at $Re_\theta = 175$. By decomposing the dynamics into scale-specific contributions, we show that distinct frequency bands dominate different streamwise stages of transition. This scale-resolved view offers guidance on where and at which frequencies external excitation may be most effective for manipulating specific phases of the transition process.

Transition proceeds through successive stages. This process involves linear and nonlinear mechanisms transferring energy from large scales to small scales. In the initial stage, disturbance amplification is governed by large, large-scale flapping of the separated shear layer, which establishes the conditions for instability and initiates roll-up. In the second stage, primary turbulent kinetic energy production occurs at the fundamental shedding scale during formation of the wall-attached roller. In the third stage, energy is redistributed to superharmonic scales as the Λ-vortices organize into aligned rows, marking the onset of harmonic amplification. Subsequently, subharmonic components and triple-correlation-driven inter-scale transfer promote broadband redistribution, leading to the breakdown of Λ-vortices and the emergence of streaky structures. In the final stage, these streaky structures extend upstream through pressure-mediated interactions and couple with newly shed Λ-vortices, contributing to their destabilization and reinforcing a self-sustaining wall-cycle-like process characteristic of fully developed turbulence.

REFERENCES

Cantwell, C. D., Moxey, D., Comerford, A., Bolis, A., Rocco, G., Mengaldo, G., De Grazia, D., Yakovlev, S., Lombard, J.-E., Ekelschot, D., Jordi, B., Xu, H., Mohamied, Y., Eskilsson, C., Nelson, B., Vos, P., Biotto, C., Kirby, R. M. & Sherwin, S. J. 2015 Nektar++: An open-source spectral/hp element framework. *Computer Physics Communications* **192**, 205–219.

Hassanpour, Maziyar, Martinuzzi, Robert J. & Piomelli, Ugo 2025 Characterization of wake-induced transition in a boundary layer. *Phys. Rev. Fluids* **10**, 124604.

Jaroslawski, Tomek, Forte, Maxime, Vermeersch, Olivier, Moschetta, Jean-Marc & Gowree, Erwin R. 2023 Disturbance growth in a laminar separation bubble subjected to free-stream turbulence. *Journal of Fluid Mechanics* **956**, A33.

Jiménez, Javier & Pinelli, Alfredo 1999 The autonomous cycle of near-wall turbulence. *Journal of Fluid Mechanics* **389**, 335–359.

Kachanov, Y S 1994 Physical mechanisms of laminar-boundary-layer transition. *Annual Review of Fluid Mechanics* **26** (Volume 26, 1994), 411–482.

Najjar, F. M. & Balachandar, S. 1998 Low-frequency unsteadiness in the wake of a normal flat plate. *Journal of Fluid Mechanics* **370**, 101–147.

Noack, Bernd R., Morzyński, Marek & Tadmor, Gilead 2011 *Reduced-Order Modelling for Flow Control*, *CISM International Centre for Mechanical Sciences*, vol. 528. Springer.

Percival, Donald B. & Walden, Andrew T. 2000 *Wavelet Methods for Time Series Analysis*, *Cambridge Series in Statistical and Probabilistic Mathematics*, vol. 4. Cambridge: Cambridge University Press.

Spalart, Philippe R. & Strelets, Michael Kh. 2000 Mechanisms of transition and heat transfer in a separation bubble. *Journal of Fluid Mechanics* **403**, 329–349.

Waleffe, Fabian 1997 On a self-sustaining process in shear flows. *Physics of Fluids* **9** (4), 883–900.